Controllable Andreev Bound States in Bilayer Graphene Josephson Junctions from Short to Long Junction Limits

Geon-Hyoung Park,[1] Wonjun Lee,[1,2] Sein Park,[1] Kenji Watanabe,[3] Takashi Taniguchi,[4] Gil Young Cho,[1,2,5] and Gil-Ho Lee[1,5,*]

[1]Deparment of Physics, Pohang University of Science and Technology, Pohang, Republic of Korea
[2]Center for Artificial Low Dimensional Electronic Systems, Institute for Basic Science, Pohang, Republic of Korea
[3]Research Center for Electronic and Optical Materials, National Institute for Materials Science, 1-1 Namiki, Tsukuba 305-0044, Japan
[4]Research Center for Materials Nanoarchitectonics, National Institute for Materials Science, 1-1 Namiki, Tsukuba 305-0044, Japan
[5]Asia Pacific Center for Theoretical Physics, Pohang, Republic of Korea

(Received 5 December 2023; revised 20 February 2024; accepted 2 April 2024; published 30 May 2024)

We demonstrate that the mode number of Andreev bound states in bilayer graphene Josephson junctions can be modulated by controlling the superconducting coherence length *in situ*. By exploiting the quadratic band dispersion of bilayer graphene, we control the Fermi velocity and thus the coherence length via the application of electrostatic gating. Tunneling spectroscopy of the Andreev bound states reveals a crossover from short to long Josephson junction regimes as we approach the charge neutral point of the bilayer graphene. Furthermore, analysis of different mode numbers of the Andreev energy spectrum allows us to estimate the phase-dependent Josephson current quantitatively. Our Letter provides a new way for studying multimode Andreev levels by tuning the Fermi velocity.

DOI: 10.1103/PhysRevLett.132.226301

In a superconductor-normal material-superconductor (SNS) Josephson junction (JJ), Cooper pairs can be transferred from one superconductor to another via the normal channel as coherently coupled electron-hole pairs generated by consecutive Andreev reflections at the SN interfaces [1–3]. Standing waves of Andreev pairs in the normal channel form Andreev bound states (ABS), which play a key role in governing the physics of SNS junctions. Recently, there has been growing interest in ABS in topological superconductivity research [4–6], quantum information processing [7–9], quantum states manipulation [10–12], and characterizing the topology of the Fermi sea [13,14].

ABS come in pairs at positive and negative energies due to the particle-hole symmetry of the superconductivity, and their energies oscillate periodically with the macroscopic superconducting phase difference between the two superconductors of the JJ. The number of ABS is determined by the ratio between the superconducting coherence length (ξ_0) and channel length (L). For a ballistic conductor, the superconducting coherence length is given by the Fermi velocity v_F and the superconducting gap Δ as $\xi_0 = \hbar v_F/2\Delta$, and it determines the short ($L \ll \xi_0$) or long ($L \gg \xi_0$) junction limit [3,15]. Conventionally, short junctions have one ABS pair and long junctions have two or more. ABS in short junctions have been observed by tunneling spectroscopy in various systems, such as two-dimensional electron gas (2DEG) systems [16,17], carbon nanotubes [18], semiconducting nanowires [19–22], and monolayer graphene [23–26], while only a few studies have observed ABS in long junctions [27,28]. Moreover, there have been no systematic attempts to verify the relationship between the number of ABS pairs and the ratio L/ξ_0. To study ABS in different junction limits in more detail, we propose a new system that allows *in situ* control of ξ_0 while simultaneously observing ABS.

In this Letter, we adopted bilayer graphene (BLG) as a normal weak link in an SNS JJ to study the crossover between short and long junction limits by controlling ξ_0. The low-energy bands of BLG exhibit approximately quadratic dispersion $E \approx p^2/2m_e^*$ at small momentum [29], so the Fermi velocity is given by $v_F = (1/\hbar)(\partial E/\partial k_F) = (\hbar\sqrt{\pi n}/m_e^*)$, where m_e^* is the effective mass of an electron, and n is the carrier density. We used *in situ* electrostatic gating to control v_F, and hence ξ_0. Note that monolayer graphene was not considered for our Letter due to its linear dispersion, which has a constant v_F.

In a microscopic mechanism of Josephson coupling, electrons and Andreev-reflected holes go through consecutive Andreev reflections at the superconducting contacts and transport Cooper pairs from one superconductor to the other [Fig. 1(a)]. This round-trip of quasiparticles results in bound states, which are called ABS. The ABS follows the Bohr-Sommerfeld quantization rule [2]:

$$2\cos^{-1}\left(\frac{E}{\Delta}\right) + \left(\frac{L}{\xi_0}\right)\left(\frac{E}{\Delta}\right) \pm \varphi = 2\pi N,$$

where $\varphi = \varphi_L - \varphi_R$ is the superconducting phase difference between the left (L) and right (R) superconductors,

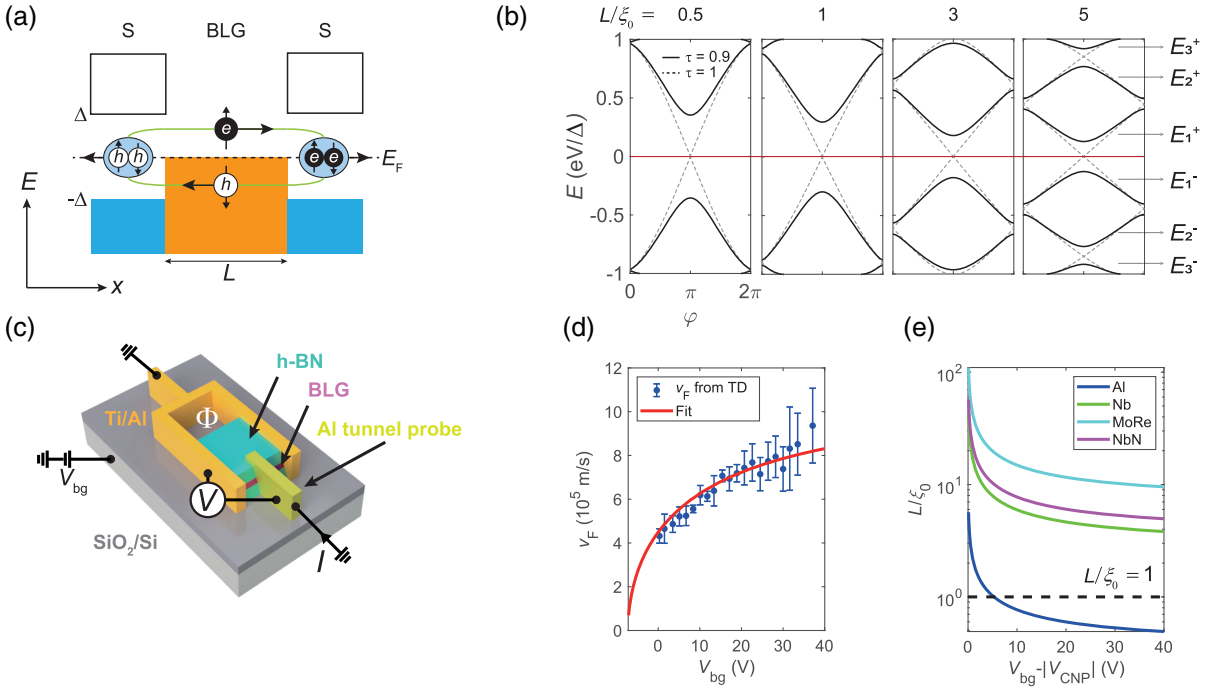

FIG. 1. (a) A schematic of Andreev bound states (ABS). (b) Energy-phase relationship of ABS at various ratios between the junction length L and the superconducting coherence length ξ_0. (c) A schematic of a loop-type Josephson junction device (LD) with the measurement configuration. (d) Backgate voltage (V_{bg}) dependence of the Fermi velocity (v_F) estimated from the Shubnikov–de Haas oscillation from two-terminal type JJ devices [TD; see Fig. S1(a) in Supplemental Material [33]]. (e) Backgate voltage dependence of L/ξ_0 calculated for different superconducting materials with v_F from (d) and $L = 1$ μm.

and N is an integer. This relation can be modified with a scatterer in the normal channel with transparency τ [30,31]. In a short junction limit, the energy-phase relationship of ABS is simply described as $E_1^{\pm} = \pm\Delta\sqrt{1-\tau\sin^2(\varphi/2)}$ [30,32]. In a long junction limit, however, there is no analytic expression for the ABS energy.

We fabricated two types of JJs: one with a superconducting loop for biasing the superconducting phase difference (LD) and the other for biasing current through the device (TD), both having the same length ($L = 1$ μm) and width ($W = 1.5$ μm) [see Fig. S1(a) in the Supplemental Material [33]]. First, we encapsulated BLG in between two hexagonal boron nitride (h-BN) sheets to protect the BLG from any chemical impurities during nanofabrication [60]. Then, 70-nm-thick Al superconducting electrodes together with a 6-nm-thick Ti adhesion layer were deposited onto the freshly etched edge of the BLG [34,60]. Lastly, superconducting side tunnel contacts were made with the deposition of 70-nm-thick Al electrodes on the edge of the BLG. When Al contacts graphene directly, a potential barrier should form between the Al and graphene [25,61], so that only quantum tunneling can occur at a low temperature. Tunneling conductance was measured by biasing the current I and measuring the voltage difference V between the tunneling probe and superconducting loop, as depicted in Fig. 1(c). The backgate voltage V_{bg} was applied to BLG via a 300-nm-thick SiO_2 dielectric layer and 26-nm-thick bottom h-BN layer to modulate the carrier density and Fermi velocity of quasiparticles in the BLG. The data were all measured at $T = 17$ mK, except Fig. S7 in the Supplemental Material [33].

Modulation of the Fermi velocity was confirmed from the temperature dependence of the Shubnikov–de Haas oscillation (SdHO) measured at the device TD. The device TD shares the same BLG as the device LD for consistency in quality. The SdHO amplitude was fitted to the Lifshitz-Kosevich formula [42,43] from temperature $T = 1.5$ to 50 K to estimate the effective mass m_e^* of quasiparticles in BLG. With quadratic energy dispersion of BLG, the Fermi velocity $v_F = \hbar k_F/m_e^*$ was calculated as a function of V_{bg} and fitted to the theoretical model as shown in Fig. 1(d) (see Figs. S3–4 in the Supplemental Material [33]) [29,62]. The charge neutral point (CNP) at $V_{bg} = -7.2$ V was determined from the two-terminal resistance as a function of V_{bg} of the device TD, which was also adopted for the CNP of the device LD. With the estimated v_F, we also calculated L/ξ_0 as a function of V_{bg} assuming various kinds of superconductor with $L = 1$ μm [Fig. 1(e)]. As BLG is in a ballistic limit away from the CNP, we used the relation $\xi_0 = \hbar v_F/2\Delta$ [see Fig. S2(b) in the Supplemental

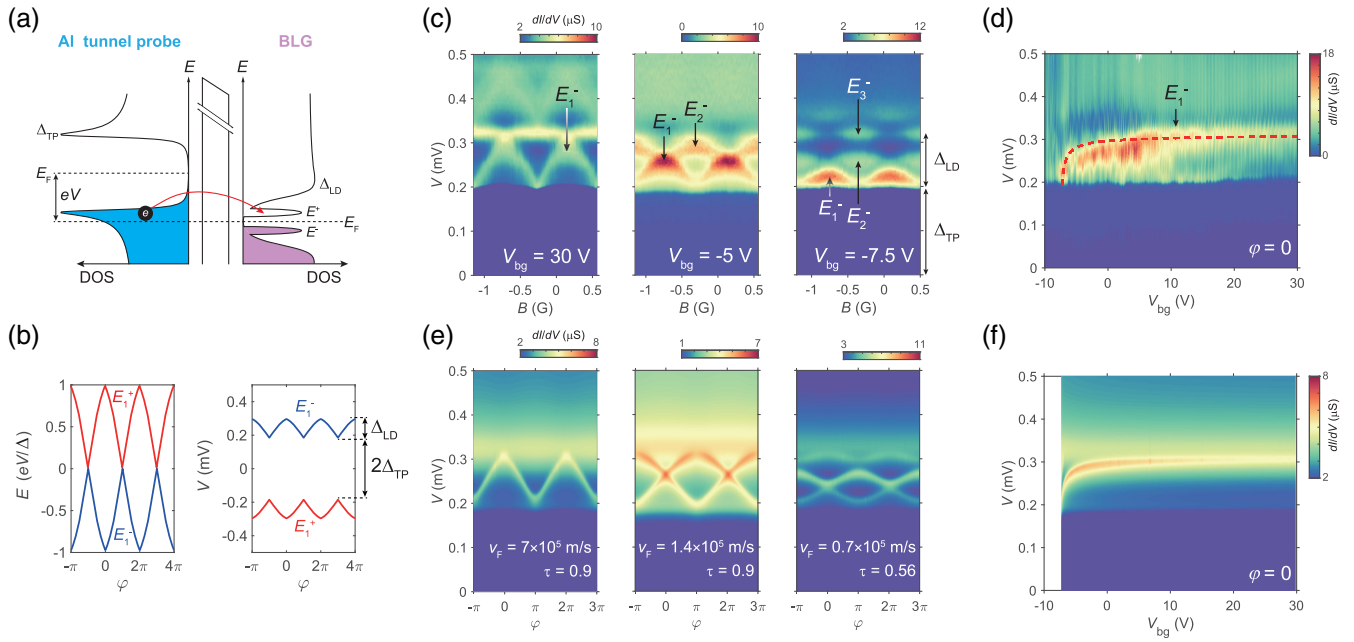

FIG. 2. (a) Elastic tunneling of an electron from a superconducting tunneling probe to the Andreev bound state in bilayer graphene (BLG) when $eV = \Delta_{TP} + E^+$. (b) (Left panel) Phase (φ) dependence of the upper (red line) and lower (blue line) ABS energies in a short junction limit with perfect transparency. (Right panel) Expected tunneling conductance (dI/dV) peak voltage V as a function of φ. (c) Color plots of dI/dV as a function of the bias voltage V and magnetic field B for different backgate voltages V_{bg} measured in device LD. (d) A color map of dI/dV as a function of the bias voltage (V) and V_{bg} at fixed $\varphi = 0$. The red dashed curve represents E_1^- theoretically calculated from (f). (e)–(f) Theoretical simulations for (c)–(d) with L/ξ_0 obtained from device TD, respectively.

Material [33]]. Since the maximum V_{bg} before the dielectric breakdown of the SiO_2 layer is around 100 V, Al has the right size of superconducting gap ($\Delta = 129$ μeV) to observe the crossover from the short to long junction limit.

Tunneling spectroscopy has recently been applied to graphene-based devices with normal [23,24] and superconducting [16,18,25,63] tunneling probes. The superconducting tunneling probe allows higher spectroscopy energy resolution than using a normal probe due to the sharp density of states (DOS) peaks near the superconducting gap edges. With the biased energy $eV = \Delta_{TP} + E^+$, as depicted in Fig. 2(a), the filled DOS peak of the probe (denoted by Δ_{TP}) aligns with the empty DOS peak of the upper ABS (denoted by E^+), where a tunneling differential conductance (dI/dV) peak is expected. The dI/dV peak does not simply represent the DOS of ABS, but it is determined by the convolution of the DOS of the probe and that of the sample [16,18,25,26]. Figure 2(b) shows the phase dependence of the ABS energy and expected dI/dV peak positions that are offset by Δ_{TP}. Figure 2(c) shows color maps of dI/dV as a function of V and φ at $V_{bg} = 30$, -5, and -7.5 V (left to right). The amplitude of the modulation of the dI/dV peaks with φ corresponds to the induced gap $\Delta_{LD} = 129$ μeV, and the offset of the modulation corresponds to the gap energy of the tunnel probe $\Delta_{TP} = 185$ μeV. The superconducting phase difference $\varphi = 2\pi\Phi/\Phi_0 = 2\pi(B - B_0)A/\Phi_0$ was controlled by external magnetic field B, with loop area A and magnetic flux quantum Φ_0. The offset $B_0 = -0.72$ G is determined by considering the center of the Fraunhofer diffraction pattern of the device TD (see Fig. S2 in the Supplemental Material [33]). The ABS oscillation period is 0.86 G, which is consistent with $\Phi_0/A = 0.85$ G with $A \sim 24$ μm^2.

By tuning the gate voltages, we observed crossover from the short to long junction limit. At $V_{bg} = 30$ V, there is only one ABS pair ($N = 1$) oscillating within the gap Δ_{LD}, which indicates that the junction is in the short junction limit. This is consistent with the expectation of $L/\xi_0 \sim 0.5$ being smaller than 1. As the gate voltage approaches V_{CNP}, the second ($N = 2$) and third ($N = 3$) ABS pairs gradually appear, and the amplitude of the dI/dV peak oscillation decreases. At $V_{bg} = -5$ V, the second ABS (E_2^-), which oscillates out-of-phase with the first ABS (E_1^-), is clearly seen. Near the CNP ($V_{bg} = -7.5$ V), the third ABS (E_3^-) starts to appear and the oscillation amplitude becomes very small. We could not observe ABS pairs with $N \geq 4$ due to the limited energy resolution. Nonetheless, adopting larger gap superconductors such as TaN (0.7 meV) [64], Nb (1 meV) [35,65,66], or MoRe (1.4 meV) [34,67] might be a viable approach to study higher modes of ABS. We also measured the gate voltage dependence of dI/dV at a fixed

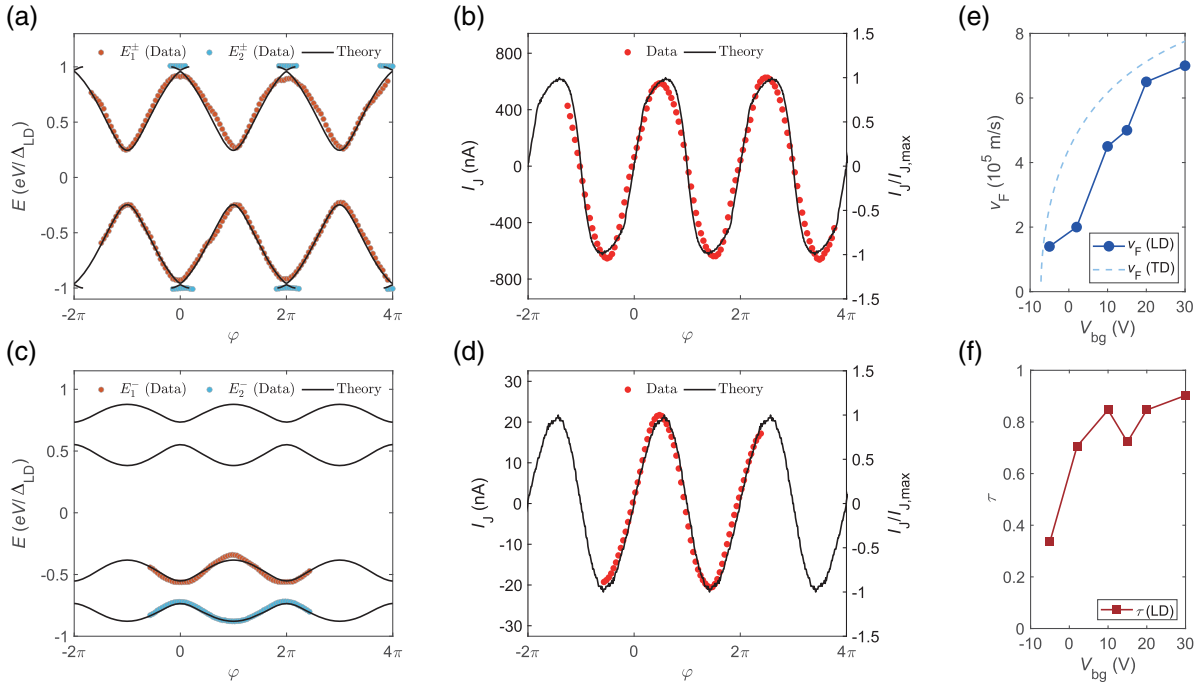

FIG. 3. (a),(c) Phase (φ) dependence of the ABS energies extracted from the dI/dV peaks at $V_{\mathrm{bg}} = 30$ and -5 V, respectively (Data). Solid black curves are theoretical fits (Theory). (b),(d) Current-phase relations calculated from the ABS energies in (a) and (c), respectively. (e) Comparison of the Fermi velocities in devices LD and TD as a function of V_{bg}. (f) Transparency τ of device LD as a function of V_{bg}.

phase difference $\varphi = 0$ to clarify the variance in E_1^-, as shown in Fig. 2(d). The positions of the dI/dV peak (E_1^-) gradually decrease as V_{bg} approaches V_{CNP}. The decrease becomes noticeable at $V_{\mathrm{bg}} < 5$ V, indicating the increase in L/ξ_0 beyond unity.

For more quantitative analysis, we introduced a theoretical model for ABS considering the geometrical asymmetry of the tunnel contact as an effective scatterer (see the Sec. S6 in the Supplemental Material [33]). The numerical simulation on ABS [Figs. 2(e) and 2(f)] using the v_{F} value obtained in the device TD [red solid line in Fig. 1(e)], and the transparency $\tau = 0.56$–0.9, successfully demonstrate the decrease in ABS energy and reduction in oscillation amplitude near the CNP. Our simulation results also explain the energy gaps between E_2^- and E_3^- at $\varphi = \pi N$ in Figs. 2(c) and 2(e), which occur due to the low transparency near the CNP [30,31]. However, the dI/dV peaks at $V_{\mathrm{bg}} < 10$ V are located at a slightly lower bias voltage and are broader than the theoretical peaks. This can be understood as the mean free path (l_{m}) of the BLG becoming shorter than the channel length when the carrier density approaches the CNP. This demands that the superconducting coherence length in a diffusive limit $\xi_0 = \sqrt{\hbar D/\Delta}$ be much shorter than ξ_0 in a ballistic limit, resulting in the increase in L/ξ_0. Here, $D = v_{\mathrm{F}} l_m/2$ is the Einstein diffusion coefficient.

The current-phase relationship (CPR) can reveal more characteristics of the Josephson supercurrent. In a zero-temperature limit, the Josephson current can be obtained by summing the contributions from the N^{th} ABS that are filled below the Fermi level, $I_{\mathrm{J}} = \sum_N I_N$, where $I_N = -(2e/h) \times (\partial E_N^-/\partial\varphi)$. From this, we can estimate the Josephson current of the junction by extracting E_N^- from the data for the short ($N = 1$) and long ($N \geq 2$) junction limits. We obtained ABS energies using the approximation $E_N^- \sim -(eV_{\mathrm{ABS},N}^- - \Delta_{\mathrm{TP}})$ instead of performing a deconvolution of the measured dI/dV. Here, $eV_{\mathrm{ABS},N}^-$ represents the bias energy at which the dI/dV peak occurs by the ABS below the Fermi level. From the extracted E_N^-, one can derive the phase dependence of I_{J} in the junction [18,23].

Figure 3(a) shows the extracted $E_N^{\pm}$ at $V_{\mathrm{bg}} = 30$ V and their theoretical fits with $L/\xi_0 = 0.56$ and $\tau = 0.9$. In Fig. 3(b), the calculated I_{J} (denoted as Data) from $E_N^{\pm}$ also shows good agreement with the theory [calculated from the theoretical fit in Fig. 3(a)]. The oscillation of I_{J} mainly follows E_1^-, since E_2^- is not dominant here ($I_{\mathrm{J}} \sim I_1$). From L/ξ_0 and τ, we can deduce that the device LD at $V_{\mathrm{bg}} = 30$ V is indeed in the short junction and ballistic limit. In comparison, Figs. 3(c) and 3(d) show the case when E_2^- is also dominant ($V_{\mathrm{bg}} = -5$ V). The theoretical calculations fit the data well with $L/\xi_0 = 2.79$ and $\tau = 0.37$, indicating that the junction is in the long junction. In Fig. 3(d), I_1 is

mostly canceled out by I_2, which oscillates in antiphase to I_1, resulting in the suppressed I_J. This indicates that the total Josephson current decreases as N increases, and it also oscillates when N is even or odd. To quantify the I_J in Figs. 3(b) and 3(d), the number of conduction channels in BLG $M \sim 2W/\lambda_F$ was also considered, where λ_F is the Fermi wavelength of electrons. M can vary from ~ 60 to 260 with V_{bg} ranging from -5 to 30 V. At $V_{bg} = -5$ V, the full participation of E_2^- strongly suppresses the total Josephson current, even considering the fourfold reduction in the channel number.

Analyzing CPR in monolayer graphene and 2DEG-based JJs has been important for verifying the τ of the junction [16,23]. In our BLG JJ, the Fermi velocity is also important as a fitting parameter, allowing us to reconfirm the variation in ξ_0 in the device LD. Figure 3(e) compares the two Fermi velocities estimated for each TD [the fitted v_F in Fig. 1(e)] and LD. Note that the two v_F estimated for both devices show a similar trend depending on V_{bg}. In Fig. 3(f), the transparency τ in the device LD also has strong dependence on the gate voltage, especially near the CNP, suggesting that Andreev pairs are affected by inhomogeneous electron-hole puddles in the BLG channels, as we discussed in Fig. 2.

In conclusion, we achieved *in situ* control of the ABS number by exploiting the parabolic energy bands of BLG as a weak link in the JJ. Modulating the carrier density from far to near the CNP, L/ξ_0 was varied from 0.5 to 5 without changing the channel length or replacing the superconducting material. The gate dependence of the tunneling conductance showed short-to-long junction crossover in a single device, demonstrating that the ABS number varies according to L/ξ_0. In the CPR analysis, precise Fermi velocity and transparency values were extracted, and it was shown that the even pairs of ABS strongly suppress the Josephson current. This Letter provides new possibilities in Andreev–multilevel physics by tuning the Fermi velocity.

This work was supported by National Research Foundation (NRF) Grants (No. 2021R1A6A1A10042944, No. 2022M3H4A1A04074153, No. RS-2023-00207732, No. RS-2023-00208291, No. 2023M3K5A1094810, No. 2023M3K5A1094813) and ITRC program (IITP-2022-RS-2022-00164799) funded by the Ministry of Science and ICT, the Air Force Office of Scientific Research under Award No. FA2386-22-1-4061, Institute of Basic Science under project code IBS-R014-D1, Samsung Science and Technology Foundation under Project (No. SSTF-BA2101-06 and No. SSTF-BA2002-05), and Samsung Electronics Co., Ltd. (IO201207-07801-01). G.-H. P. was supported by the Basic Science Research Institute Fund (Grant No. 2021R1A6A1A10042944). K. W. and T. T. acknowledge support from the JSPS KAKENHI (Grants No. 21H05233 and No. 23H02052) and World Premier International Research Center Initiative (WPI), MEXT, Japan.

*To whom all correspondence should be addressed: lghman@postech.ac.kr

[1] A. F. Andreev, Sov. Phys. JETP **19**, 1228 (1964).
[2] I. O. Kulik, Sov. Phys. JETP **30**, 944 (1970).
[3] K. K. Likharev, Rev. Mod. Phys. **51**, 101 (1979).
[4] F. Pientka, A. Keselman, E. Berg, A. Yacoby, A. Stern, and B. I. Halperin, Phys. Rev. X **7**, 021032 (2017).
[5] M. Hell, M. Leijnse, and K. Flensberg, Phys. Rev. Lett. **118**, 107701 (2017).
[6] T. H. Hsieh and L. Fu, Phys. Rev. Lett. **108**, 107005 (2012).
[7] A. Zazunov, V. S. Shumeiko, E. N. Bratus', J. Lantz, and G. Wendin, Phys. Rev. Lett. **90**, 087003 (2003).
[8] C. Janvier *et al.*, Science **349**, 1199 (2015).
[9] L. Bretheau, Ç. Ö. Girit, H. Pothier, D. Esteve, and C. Urbina, Nature (London) **499**, 312 (2013).
[10] J. J. A. Baselmans, A. F. Morpurgo, B. J. van Wees, and T. M. Klapwijk, Nature (London) **397**, 43 (1999).
[11] N. M. Chtchelkatchev and Y. V. Nazarov, Phys. Rev. Lett. **90**, 226806 (2003).
[12] E. Strambini, S. D'Ambrosio, F. Vischi, F. S. Bergeret, Y. V. Nazarov, and F. Giazotto, Nat. Nanotechnol. **11**, 1055 (2016).
[13] P. M. Tam and C. L. Kane, Phys. Rev. Lett. **130**, 096301 (2023).
[14] P. M. Tam, C. De Beule, and C. L. Kane, Phys. Rev. B **107**, 245422 (2023).
[15] I. V. Borzenets *et al.*, Phys. Rev. Lett. **117**, 237002 (2016).
[16] F. Nichele *et al.*, Phys. Rev. Lett. **124**, 226801 (2020).
[17] C. M. Moehle, P. K. Rout, N. A. Jainandunsing, D. Kuiri, C. T. Ke, D. Xiao, C. Thomas, M. J. Manfra, M. P. Nowak, and S. Goswami, Nano Lett. **22**, 8601 (2022).
[18] J. D. Pillet, C. H. L. Quay, P. Morfin, C. Bena, A. L. Yeyati, and P. Joyez, Nat. Phys. **6**, 965 (2010).
[19] W. Chang, V. E. Manucharyan, T. S. Jespersen, J. Nygård, and C. M. Marcus, Phys. Rev. Lett. **110**, 217005 (2013).
[20] D. J. van Woerkom, A. Proutski, B. van Heck, D. Bouman, J. I. Väyrynen, L. I. Glazman, P. Krogstrup, J. Nygård, L. P. Kouwenhoven, and A. Geresdi, Nat. Phys. **13**, 876 (2017).
[21] A. Pöschl, A. Danilenko, D. Sabonis, K. Kristjuhan, T. Lindemann, C. Thomas, M. J. Manfra, and C. M. Marcus, Phys. Rev. B **106**, L241301 (2022).
[22] A. Pöschl, A. Danilenko, D. Sabonis, K. Kristjuhan, T. Lindemann, C. Thomas, M. J. Manfra, and C. M. Marcus, Phys. Rev. B **106**, L161301 (2022).
[23] L. Bretheau, J. I.-J. Wang, R. Pisoni, K. Watanabe, T. Taniguchi, and P. Jarillo-Herrero, Nat. Phys. **13**, 756 (2017).
[24] J. I.-J. Wang, L. Bretheau, D. Rodan-Legrain, R. Pisoni, K. Watanabe, T. Taniguchi, and P. Jarillo-Herrero, Phys. Rev. B **98**, 121411(R) (2018).
[25] S. Park, W. Lee, S. Jang, Y.-B. Choi, J. Park, W. Jung, K. Watanabe, T. Taniguchi, G. Y. Cho, and G.-H. Lee, Nature (London) **603**, 421 (2022).

[26] T. Dirks, T. L. Hughes, S. Lal, B. Uchoa, Y.-F. Chen, C. Chialvo, P. M. Goldbart, and N. Mason, Nat. Phys. **7**, 386 (2011).
[27] L. Tosi, C. Metzger, M. F. Goffman, C. Urbina, H. Pothier, S. Park, A. L. Yeyati, J. Nygård, and P. Krogstrup, Phys. Rev. X **9**, 011010 (2019).
[28] P. Zellekens, R. S. Deacon, P. Perla, D. Grützmacher, M. I. Lepsa, T. Schäpers, and K. Ishibashi, Commun. Phys. **5**, 267 (2022).
[29] E. McCann and M. Koshino, Rep. Prog. Phys. **76**, 056503 (2013).
[30] P. F. Bagwell, Phys. Rev. B **46**, 12573 (1992).
[31] P. Samuelsson, J. Lantz, V. S. Shumeiko, and G. Wendin, Phys. Rev. B **62**, 1319 (2000).
[32] C. W. J. Beenakker, Phys. Rev. Lett. **67**, 3836 (1991).
[33] See Supplemental Material at http://link.aps.org/supplemental/10.1103/PhysRevLett.132.226301, which includes Refs. [34–59] for details on the experiment and the numerical simulation of ABS.
[34] V. E. Calado, S. Goswami, G. Nanda, M. Diez, A. R. Akhmerov, K. Watanabe, T. Taniguchi, T. M. Klapwijk, and L. M. K. Vandersypen, Nat. Nanotechnol. **10**, 761 (2015).
[35] M. Ben Shalom *et al.*, Nat. Phys. **12**, 318 (2016).
[36] J. Park, J. H. Lee, G.-H. Lee, Y. Takane, K.-I. Imura, T. Taniguchi, K. Watanabe, and H.-J. Lee, Phys. Rev. Lett. **120**, 077701 (2018).
[37] C. Handschin, P. Makk, P. Rickhaus, M.-H. Liu, K. Watanabe, T. Taniguchi, K. Richter, and C. Schönenberger, Nano Lett. **17**, 328 (2017).
[38] H. B. Heersche, P. Jarillo-Herrero, J. B. Oostinga, L. M. K. Vandersypen, and A. F. Morpurgo, Nature (London) **446**, 56 (2007).
[39] D. Jeong, J.-H. Choi, G.-H. Lee, S. Jo, Y.-J. Doh, and H.-J. Lee, Phys. Rev. B **83**, 094503 (2011).
[40] V. Barzykin and A. M. Zagoskin, Superlattices Microstruct. **25**, 797 (1999).
[41] A. Laturia, M. L. Van de Put, and W. G. Vandenberghe, NPJ 2D Mater. Appl. **2**, 6 (2018).
[42] K. Zou, X. Hong, and J. Zhu, Phys. Rev. B **84**, 085408 (2011).
[43] J. Li, L. Z. Tan, K. Zou, A. A. Stabile, D. J. Seiwell, K. Watanabe, T. Taniguchi, S. G. Louie, and J. Zhu, Phys. Rev. B **94**, 161406(R) (2016).
[44] J. W. McClure, Phys. Rev. **108**, 612 (1957).
[45] J. C. Slonczewski and P. R. Weiss, Phys. Rev. **109**, 272 (1958).
[46] J. W. McClure, Phys. Rev. **119**, 606 (1960).
[47] C. W. J. Beenakker, Phys. Rev. Lett. **97**, 067007 (2006).
[48] G. B. Lesovik and I. A. Sadovskyy, Phys. Usp. **54**, 1007 (2011).
[49] M. Barbier, P. Vasilopoulos, and F. M. Peeters, Phys. Rev. B **82**, 235408 (2010).
[50] S. Pinon, V. Kaladzhyan, and C. Bena, Phys. Rev. B **101**, 205136 (2020).
[51] J. A. Sauls, Phil. Trans. R. Soc. A **376**, 20180140 (2018).
[52] M. Titov and C. W. J. Beenakker, Phys. Rev. B **74**, 041401 (R) (2006).
[53] T. Ludwig, Phys. Rev. B **75**, 195322 (2007).
[54] I. Snyman and C. W. J. Beenakker, Phys. Rev. B **75**, 045322 (2007).
[55] J. Bardeen, L. N. Cooper, and J. R. Schrieffer, Phys. Rev. **108**, 1175 (1957).
[56] F. Gross, B. S. Chandrasekhar, D. Einzel, K. Andres, P. J. Hirschfeld, H. R. Ott, J. Beuers, Z. Fisk, and J. L. Smith, Z. Phys. B **64**, 175 (1986).
[57] J. Lantz, V. S. Shumeiko, E. Bratus, and G. Wendin, Phys. Rev. B **65**, 134523 (2002).
[58] J. M. Rowell and W. L. McMillan, Phys. Rev. Lett. **16**, 453 (1966).
[59] B. W. Heinrich, L. Braun, J. I. Pascual, and K. J. Franke, Nat. Phys. **9**, 765 (2013).
[60] L. Wang *et al.*, Science **342**, 614 (2013).
[61] G.-H. Lee, S. Kim, S.-H. Jhi, and H.-J. Lee, Nat. Commun. **6**, 6181 (2015).
[62] E. McCann and V. I. Fal'ko, Phys. Rev. Lett. **96**, 086805 (2006).
[63] M. Meschke, J. T. Peltonen, J. P. Pekola, and F. Giazotto, Phys. Rev. B **84**, 214514 (2011).
[64] M. Müller, R. Hoepfl, L. Liensberger, S. Geprägs, H. Huebl, M. Weiler, R. Gross, and M. Althammer, Mater. Quantum. Technol. **1**, 045001 (2021).
[65] P. Rickhaus, M. Weiss, L. Marot, and C. Schönenberger, Nano Lett. **12**, 1942 (2012).
[66] G.-H. Park, M. Kim, K. Watanabe, T. Taniguchi, and H.-J. Lee, Sci. Rep. **7**, 10953 (2017).
[67] F. Amet *et al.*, Science **352**, 966 (2016).